LETTERS
PUBLISHED ONLINE: 14 OCTOBER 2012 | DOI: 10.1038/NMAT3443

nature materials

Nanometre optical coatings based on strong interference effects in highly absorbing media

Mikhail A. Kats, Romain Blanchard, Patrice Genevet and Federico Capasso*

Optical coatings, which consist of one or more films of dielectric or metallic materials, are widely used in applications ranging from mirrors to eyeglasses and photography lenses[1,2]. Many conventional dielectric coatings rely on Fabry–Perot-type interference, involving multiple optical passes through transparent layers with thicknesses of the order of the wavelength to achieve functionalities such as anti-reflection, high-reflection and dichroism. Highly absorbing dielectrics are typically not used because it is generally accepted that light propagation through such media destroys interference effects. We show that under appropriate conditions interference can instead persist in ultrathin, highly absorbing films of a few to tens of nanometres in thickness, and demonstrate a new type of optical coating comprising such a film on a metallic substrate, which selectively absorbs various frequency ranges of the incident light. These coatings have a low sensitivity to the angle of incidence and require minimal amounts of absorbing material that can be as thin as 5–20 nm for visible light. This technology has the potential for a variety of applications from ultrathin photodetectors and solar cells to optical filters, to labelling, and even the visual arts and jewellery.

Optical coatings are a key component of nearly every optical device, and have been extensively studied for decades[1,2]. Conventional coatings comprise some combination of thin metallic films serving as partial and full reflectors, and wavelength-scale-thick dielectric films that rely on Fabry–Perot-type or thin-film interference—the same effect that is responsible for the colourful patterns on oil films and soap bubbles and for Newton's rings. Other examples include anti-reflection and high-reflection coatings, which are often made by stacking layers of dielectrics with quarter-wave thickness ($\lambda/4n$, where n is the refractive index of the material). These interference effects rely on multi-pass light circulation within the optical cavities formed by the films, and are typically sensitive to the angle of incidence. By engineering multi-layer dielectric stacks, more complex and robust devices such as omni-directional reflectors can be created[3]. Today, optical coatings, which often comprise many aperiodic layers, are primarily designed and optimized by computer software[4]; a variety of commercial software for thin-film calculation and optimization is available, including Essential Macleod, FilmStar, Film Wizard and OptiLayer.

Here, we explore the use of highly absorptive dielectric films as optical coatings. The Fabry–Perot-type effect of conventional optical thin films uses constructive and destructive interference, with the optical phase controlled by gradual accumulation within the nearly transparent dielectric layers. The material losses in the dielectrics are usually assumed to be small such that light is absorbed gradually, if at all, and the interface reflection and transmission phase changes at the interfaces between the dielectric films can therefore be assumed to be either 0 or π, depending on the index contrast. Our approach instead uses highly absorbing dielectrics (semiconductors at photon energies above the bandgap in the present demonstration) in which light is rapidly attenuated, together with metals that have finite optical conductivity. Combining these materials gives access to a range of interface reflection and transmission phase shifts that can be engineered by modification of the material properties. The large optical attenuation within the highly absorbing dielectrics and the concomitant non-trivial interface phase shifts lead to strong resonant behaviour in films that are much thinner than the wavelength of light. We demonstrate these ultrathin coatings on the surfaces of noble metals in the visible regime and show that deposition of nanometres of a lossy dielectric on a metal results in a marked modification of the reflectivity spectrum (and therefore colour).

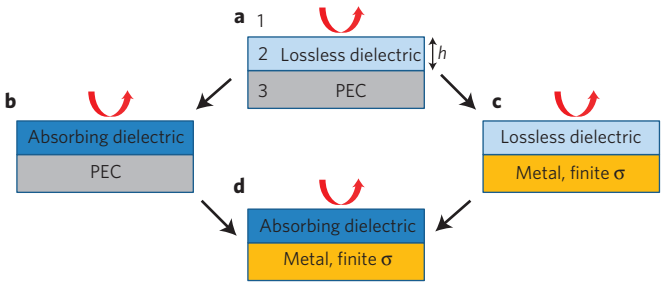

Figure 1 | Schematic of incident light from medium 1 (air) being reflected from a structure comprising dielectric medium 2 with thickness *h* and metallic medium 3. a, The case of a perfect electric conductor (PEC) and a lossless dielectric. As there is no absorption and no penetration into the metal, the reflectivity equals unity at all wavelengths. Structures approaching this limit can be used as phase-shifting elements, which are known as Gires–Tournois etalons. **b**, An absorbing dielectric on a PEC substrate supports an absorption resonance for $h \sim m\lambda/4n_2$ assuming that the losses (k_2) are relatively small and m is an odd integer. No resonance exists for h smaller than $\lambda/4n_2$. **c**, A lossless dielectric on a substrate with finite optical conductivity (for example, Au at visible frequencies) can support a resonance for $h \ll \lambda/4n_2$ owing to the non-trivial phase shifts at the interface between medium 2 and medium 3, but the total absorption is small because the only loss mechanism is the one associated with the finite reflectivity of the metal. **d**, An ultrathin ($h \ll \lambda/4n_2$) absorbing dielectric on Au at visible frequencies can support a strong and widely tailorable absorption resonance.

The equations describing the behaviour of light incident from air ($n_1 = 1$) onto a lossy film with thickness h and complex refractive index $\tilde{n}_2 = n_2 + ik_2$, deposited on a metallic substrate

School of Engineering and Applied Sciences, Harvard University, Cambridge, Massachusetts 02138, USA. *e-mail: capasso@seas.harvard.edu.

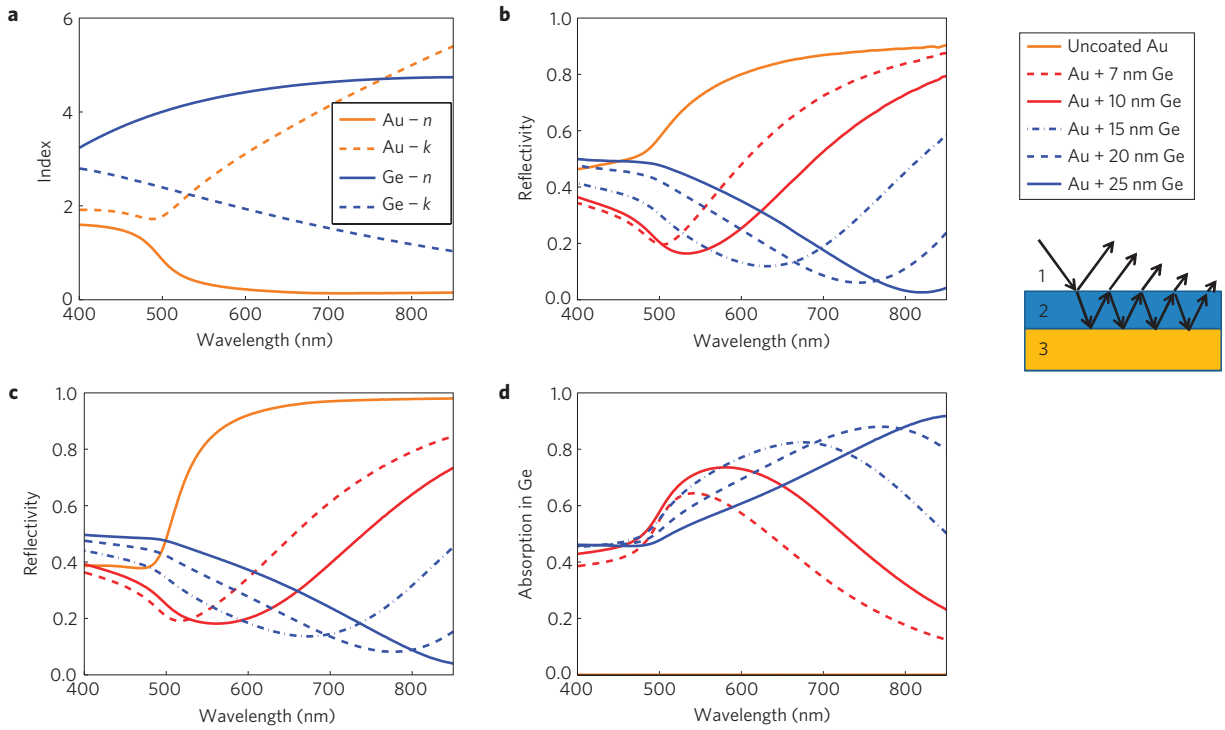

Figure 2 | Optical properties of the thin films. a, Real and imaginary parts of the complex refractive indices of Au and Ge, obtained by variable-angle spectroscopic ellipsometry. **b**, Near-normal incidence (7°) reflection spectra of thick Au coated with 7, 10, 15, 20 and 25 nm of Ge. Inset: schematic of the Ge film on a Au substrate, showing a partial wave decomposition. **c**, Calculated reflection spectra using equation (1) and the optical constants in **a** corresponding to the measurement in **b**. **d**, Calculated fraction of the total incident light that is absorbed within the Ge layer.

with complex index $\tilde{n}_3$ (Fig. 1), can be found in optics textbooks[5]. The reflection coefficient for transverse-electric (s-polarized) light incident at an angle θ_1 is

$$\tilde{r} = \frac{\tilde{r}_{12} + \tilde{r}_{23} e^{2i\tilde{\beta}}}{1 + \tilde{r}_{12}\tilde{r}_{23} e^{2i\tilde{\beta}}} \quad (1)$$

where $\tilde{r}_{mn} = (\tilde{p}_m - \tilde{p}_n)/(\tilde{p}_m + \tilde{p}_n)$, $\tilde{p}_m = \tilde{n}_m \cos(\tilde{\theta}_m)$, $\tilde{\beta} = (2\pi/\lambda)\tilde{n}_2 h \cos(\tilde{\theta}_2)$ and $\tilde{\theta}_m = \sin^{-1}(\sin(\theta_1)/\tilde{n}_m)$, which is the complex-valued form of Snell's law (pp. 740–741 of ref. 5). For transverse-magnetic (p-polarized) light, $\tilde{p}_m$ is replaced by $\tilde{q}_m = \cos(\tilde{\theta}_m)/\tilde{n}_m$. The total reflectivity is given by $R = |\tilde{r}|^2$, and because we assume that the substrate is metallic such that there is no transmission, the absorption of the structure can be written as $A = 1 - R$. One noteworthy special case of this three-layer structure is an asymmetric Fabry–Perot cavity comprising a quarter-wave film (or odd multiples thereof, such that $h \simeq m\lambda/4n_2$, where m is an odd integer) on a perfect reflector (Fig. 1a). This resonator in the presence of moderate losses serves as an absorbing optical cavity in which the loss can be considered as a perturbation. In the absence of loss, this type of cavity functions as a phase-shifting element called a Gires–Tournois etalon[6]. Asymmetric Fabry–Perot cavities have been used for reflection modulation[7], resonant cavity-enhanced photodetection and emission[8,9], ferroelectric infrared detection[10] and other applications.

For a metal substrate in the perfect electric conductor (PEC) limit, $n_3 \to \infty$ and $k_3 \to \infty$, so $\tilde{r}_{2,3} = -1$, corresponding to complete reflection with a phase shift of π (Fig. 1a,b), which makes $h \simeq \lambda/4n_2$ the lower limit on the thickness of a resonant cavity because a round trip inside such a cavity should accumulate approximately 0 phase (modulo 2π; see Supplementary Information for details). At optical frequencies, however, metals have finite conductivity and therefore their complex index is finite[5] (similar metal-like complex indices can also be found in a variety of non-metallic materials at longer wavelengths such as, for example, indium tin oxide in the near-infrared region[11], sapphire in the mid-infrared region[12] and so on), so the reflection phase shift at the metal interface can vary (Fig. 1c). Likewise, if a dielectric film has large optical losses (k_2 of the order of n_2), the reflection and transmission phase shifts at the boundary between it and air are not limited to 0 or π as in the case for lossless dielectrics (Fig. 1b,d). These non-trivial interface phase shifts allow the total phase accumulation, which includes both the interface and propagation phase shifts, to reach approximately 0 (modulo 2π) for certain films with thicknesses significantly below $\lambda/4n_2$, creating an absorption resonance (note that the phase accumulation is close to but not precisely zero at this resonance condition when the system has high losses). As there is very little light propagation in such a thin structure, the material optical losses must be very high for the round-trip absorption to be significant. By combining these non-trivial interface phase shifts, the phase accumulated through propagation and the attenuation of the wave as it propagates through the highly lossy medium, a new type of optical coating can be designed (Fig. 1d) where losses are no longer considered as a perturbation but are an integral part of the design.

We demonstrated these concepts at visible frequencies by modifying the reflectivity of a gold (Au) surface by coating it with evaporated germanium (Ge) films of a few nanometres in thickness, which creates broadband absorption resonances with the spectral position determined by the film thickness. The wide optical absorption band influences the colour by suppressing the reflectivity in a portion of the visible spectrum. Ge was selected because it is highly absorbing at visible frequencies (see Fig. 2a) owing to direct electronic transitions that appear at energies higher than that of the L-absorption edge[13]. We coated an optically thick (150 nm) Au film with Ge of thickness h between 7 and 25 nm by using electron-beam evaporation, which resulted in marked changes in the reflectivity. We performed near-normal

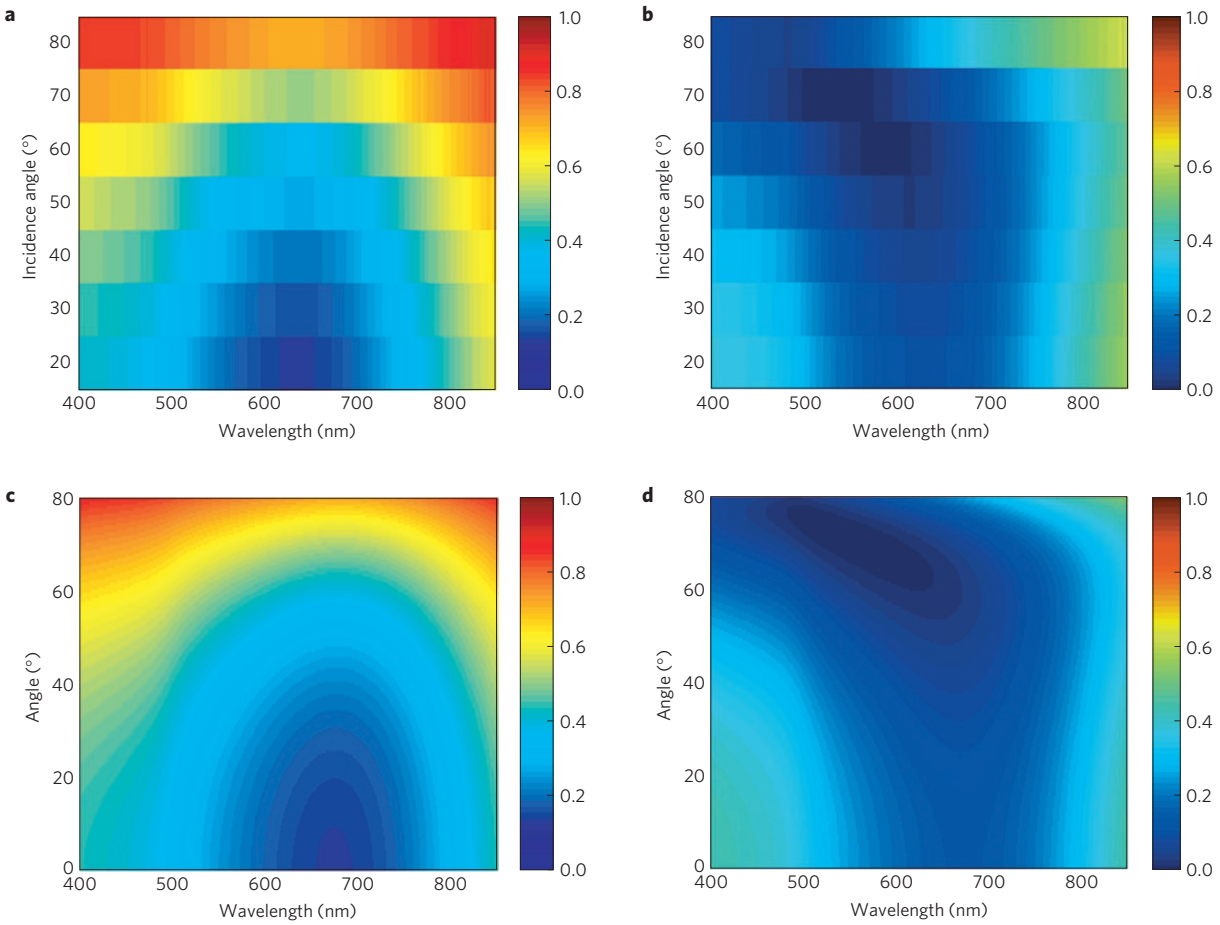

Figure 3 | Reflectivity spectra. a,**b**, Experimental reflectivity spectra for s- and p-polarization, respectively, for angles of incidence from 20° to 80° for an Au film coated with 15 nm of Ge (the value of reflectivity is indicated by the colour bars). **c**,**d**, The calculated spectra corresponding to those in **a**,**b** using equation (1).

incidence measurements (7° incidence angle with unpolarized light) between 400 and 850 nm using a spectrophotometer (see Methods and Supplementary Information for details on the sample preparation and measurement). The experimental reflectivity spectra for Ge films of thickness between 7 and 25 nm coated on Au are given in Fig. 2b.

The calculated reflection spectra corresponding to the measurements in Fig. 2b are obtained by using equation (1), and are shown in Fig. 2c. Excellent agreement is obtained between the experimental data and the calculations. The optical constants for the evaporated Au and Ge were obtained by variable-angle spectroscopic ellipsometry of optically thick films (see Supplementary Information for more details). We also computed the total fraction of the incident light that is absorbed within the Ge film (Fig. 2d), finding that most of the absorption occurs in this layer as opposed to the underlying Au. For example, in the case of the 15 nm Ge sample at a wavelength of ~670 nm, over 80% of the incident light is absorbed in the Ge layer whereas only ~4% of the light is absorbed in the Au, with the remaining ~15% of the light reflected. The spectral position of the absorption band, which corresponds to the reflectivity minimum, depends on h, with a shift of approximately 20 nm in wavelength for every 1 nm change in h across the visible spectral range. This strong absorption resonance occurs in a film that is much thinner than the wavelength of light (for example, $h \sim \lambda/(13n_2)$ at $\lambda \sim 560$ nm, with $n_2 \sim 4.3$ for the 10 nm Ge film in the calculation)—a result of the interplay between the complex reflection coefficient at the Ge/Au substrate and the large but finite attenuation of light within the Ge film (see Supplementary Information for a detailed explanation based on decomposition into partial waves). Note that in our material system, the absorption coefficient of Ge decreases with increasing wavelength and the properties of Au slowly approach those of a PEC, so the resonant absorption thickness will slowly converge to $h \sim \lambda/(4n_2)$ at long wavelengths.

As these coatings are much thinner than the wavelength of light, there is little phase accumulation due to the propagation through the film compared with the reflection phase change on reflection. As a result, the optical properties of these coatings are robust with respect to the angle of incidence. We demonstrated this by measuring the s- and p-polarized reflectivity of the sample with 15 nm of Ge, which shows that the absorption feature remains prominent for angles of incidence from 0° to ~60° in both polarizations (Fig. 3a,b). The corresponding calculated spectra are shown in Fig. 3c,d.

The large change in reflectivity allows for the colouring of metals using these films of subwavelength thickness. Figure 4 shows a photograph of samples of Au coated with Ge from 0 to 25 nm in thickness, creating a spectrum of colours including pink, blue and violet. In samples a–h, the substrate material for Au deposition was a polished silicon wafer. In samples i–k, however, the rough, unpolished back-side of the wafer was used, and the various colours are still clearly visible, indicating that the present effect is relatively insensitive to surface roughness. This is to be expected given the small dependence of the reflectivity on the incidence angle shown in Fig. 3, but runs against intuition given our everyday experience with thin-film interference effects. We also show several samples of

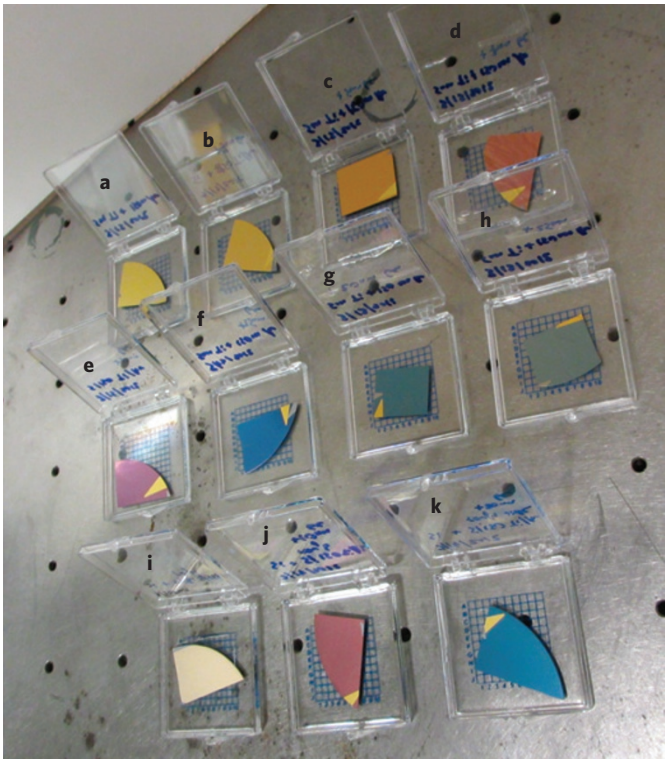

Figure 4 | Wide variety of colours formed by coating Au with nanometre films of Ge. a–h, 0, 3, 5, 7, 10, 15, 20 and 25 nm of Ge deposited on optically thick Au, which was deposited on polished silicon. The clip marks from mounting in the electron-beam evaporator are visible. **i–k**, 0, 10 and 20 nm of Ge deposited over 150 nm of Au, on a rough (unpolished) silicon substrate.

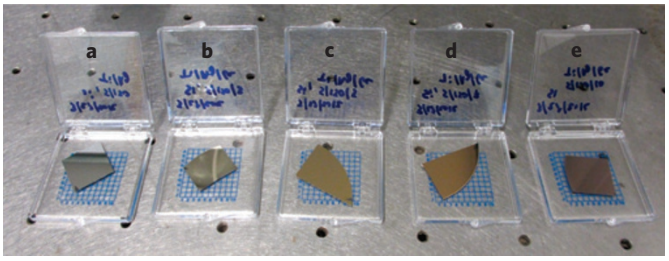

Figure 5 | Spectrum of colours resulting from coating Ag with nanometre films of Ge. a–e, Thick Ag films coated with 0, 3, 5, 7 and 10 nm of evaporated Ge, respectively.

silver (Ag) coloured using the same principle (Fig. 5); in particular, a colour similar to that of Au is induced in Ag samples by coating them with ~7 nm of Ge (Fig. 5d).

We note that the modification of the absorption and colour of metals has recently been demonstrated using nano-, micro- and macrostructuring of the metal surface by lithography and etching, femtosecond laser ablation or other methods[14–18]. By comparison, our technique is non-damaging to the metal surface, can be reversed by chemical etching of the absorbing dielectric layer, does not require any serial fabrication steps and involves only smooth surfaces, which may be advantageous for integration into devices. Furthermore, the approach demonstrated here does not involve multiple scattering, metallic nanocavity resonances or surface plasmons, as in refs 14–18, but is instead a result of simple, albeit counterintuitive, thin-film interference; this simplicity allows for the prediction and design of new coatings using simple analytical expressions such as equation (1).

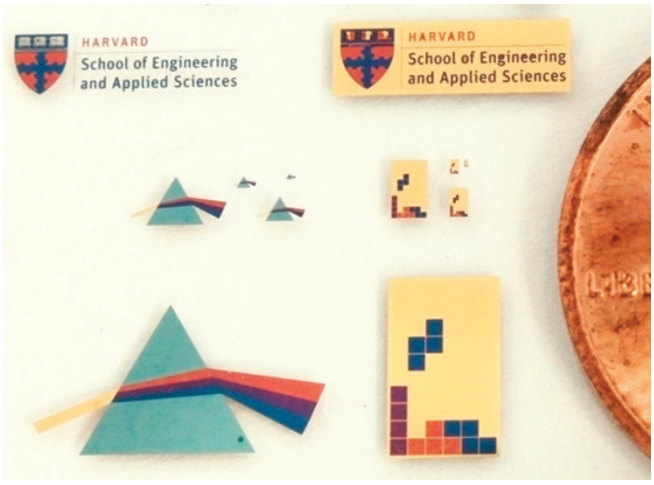

Figure 6 | Photograph of colour images generated using multi-step patterning of ultrathin Ge films, with the edge of a United States penny included for size comparison. Five steps of photolithography with alignment are used to selectively deposit an optically thick layer of Au on a glass slide, followed by Ge layers of either 7, 11, 15 or 25 nm. This yields light pink, purple, dark blue and light blue colours, respectively. Among the demonstrated patterns are the logo and shield of the School of Engineering and Applied Sciences; these are a trademark of Harvard University, and are protected by copyright; they are used in this research with permission.

In addition to continuous coatings, single- and multicolour images can be created by combining the deposition of ultrathin absorbing films with conventional lithographic techniques. As an example, we generated several colour images on a glass slide with feature sizes ranging from micrometres to millimetres by using multi-step contact photolithography with alignment (Fig. 6). Five colours are demonstrated: Au (0 nm of Ge), light pink (~7 nm), purple (~11 nm), dark blue (~15 nm) and light blue (~25 nm).

The approach of using ultrathin, absorptive dielectric films as optical coatings is very general and can be applied to applications across a range of frequencies, starting with simple absorbers and colour filters. The large change in optical properties given relatively small changes in material thickness can be used for subnanometre optical thickness monitoring of the deposition of semiconductor films. The colouring of metals with nanometre-thick films of inexpensive material may prove useful in various aspects of design and the visual arts. Furthermore, creating patterned structures comprising ultrathin absorbing coatings using conventional fabrication techniques introduces new capabilities for labelling, printing and otherwise displaying information.

The high degree of absorption in semiconductors makes them excellent candidate materials for these ultrathin coatings, potentially enabling new types of photodetectors with enhanced quantum efficiency that require orders of magnitude less semiconductor material, significantly decreasing the material cost and growth time (compared with, for example, resonant-cavity-enhanced photodetectors that have an absorbing layer inside a wavelength-scale Fabry–Perot cavity). Solar cell applications could also benefit from the large spectral bandwidth of the absorption resonances. Furthermore, in solar cells there is a tradeoff between thickness and material purity that is related to charge carrier lifetimes in materials with defects[19]; making ultrathin highly absorbing layers could relax this purity constraint, further reducing costs. Finally, when applied at infrared, millimetre and longer wavelengths, absorbing coatings backed by a reflector can be components of bolometer-type detectors and stealth technology.

Methods

The Au, Ge and Ag films were deposited by electron-beam evaporation using a Denton evaporator. Au was deposited at a rate of ~2 Å s^{-1} under a pressure of ~10^{-6} torr without substrate heating, with the rate measured by a crystal monitor. Ge was deposited at a rate of 1 Å s^{-1} at a pressure of ~2×10^{-6} torr. The images in Figs 4 and 5 were taken with a Canon PowerShot ELPH 310 HS digital camera under illumination from regular white ceiling fluorescent lights.

The near-normal incidence reflectivity spectra were taken using a Hitachi 4100 spectrophotometer with a tungsten lamp source and a photomultiplier tube in the 400–850 nm range. The angle-dependent, polarization-dependent spectra were obtained using a Woollam WVASE32 spectroscopic ellipsometer using reflection/transmission mode. The stability of these optical coatings is discussed in the Supplementary Information.

The complex refractive indices given in Fig. 2a and used in the calculation of the spectra in Figs 2c and 3c,d were obtained by variable-angle spectroscopic ellipsometry of optically thick evaporated films (150 nm for Au and 1,000 nm for Ge in the 400–850 nm range). In ellipsometry literature, this sort of measurement is referred to as measuring the pseudo-dielectric function, which is named pseudo because of the assumption that a single reflection comes from a sharp interface between the material and the air[20]. We preferred this method to ellipsometry on thin absorbing films (for example, ~10 nm Ge on a known substrate) because it decreases the number of unknowns from (n, k, h) to (n, k), which helps avoid over-fitting errors and non-unique solutions.

The theoretical spectra in Figs 2c and 3c,d were calculated using equation (1). In the case of Fig. 2c, we simulated unpolarized incident light by calculating the reflectivity for both s- and p-polarizations, and taking an average of the two.

The multicolour patterns of Fig. 6 were generated by five steps of contact photolithography with alignment. Photoresist was spun onto a glass slide (Shipley S1813, 4,000 r.p.m.), was exposed through chrome-coated glass photomasks using a Karl Suss MJB4 mask aligner and was then developed using CD-26. The Au and Ge films were then deposited through the resulting mask, with the excess material removed using liftoff in acetone with ultrasonic agitation. The deposition thicknesses were 65 nm Au (preceded by a 5 nm Ti adhesion layer) to create an optically thick layer, followed by 7 nm, 4 nm, 4 nm and 10 nm of Ge, creating overall Ge layers of thickness 7 nm, 11 nm, 15 nm and 25 nm, respectively.

Received 20 June 2012; accepted 31 August 2012; published online 14 October 2012

References

1. Macleod, H. A. *Thin-film Optical Filters* (Adam Hilger, 1986).
2. Yeh, P. *Optical Waves in Layered Media* (Wiley, 2005).
3. Fink, Y. *et al.* A dielectric omnidirectional reflector. *Science* **282,** 1679–1682 (1998).
4. Dobrowolski, J. A. Versatile computer program for absorbing optical thin film systems. *Appl. Opt.* **20,** 74–81 (1981).
5. Born, M & Wolf, E *Principles of Optics* 7th edn (Cambridge Univ. Press, 2003).
6. Gires, F. & Tournois, P. Interferometre utilisable pour la compression d'impulsions lumineuses modulees en frequence. *C. R. Acad. Sci. Paris* **258,** 6112–6615 (1964).
7. Yan, R. H., Simes, R. J. & Coldren, L. A. Electroabsorptive Fabry–Perot reflection modulators with asymmetric mirrors. *IEEE Photon. Technol. Lett.* **1,** 273–275 (1989).
8. Kishino, K., Selim Unlu, M., Chyi, J-I., Reed, J., Arsenault, L. & Morkoc, H. Resonant cavity-enhanced (RCE) photodetectors. *IEEE J. Quantum Electron.* **27,** 2025–2034 (1991).
9. Unlu, M. S. & Strite, S. Resonant cavity enhanced photonic devices. *J. Appl. Phys.* **78,** 607–639 (1995).
10. Bly, V. T. & Cox, J. T Infrared absorber for ferroelectric detectors. *Appl. Opt.* **33,** 26–30 (1994).
11. Robusto, P. F. & Braustein, R. Optical measurements of the surface plasmon of indium tin oxide. *Phys. Status Solidi* **119,** 155–168 (1990).
12. Gervais, F. & Piriou, B. Anharmonicity in several-polar-mode crystals: adjusting phonon self-energy of LO and TO modes in Al_2O_3 and TiO_2 to fit infrared reflectivity. *J. Phys. C* **7,** 2374–2386 (1974).
13. Cardona, M. & Harbeke, G. Absorption spectrum of germanium and zinc-blende-type materials at energies higher than the fundamental absorption edge. *J. Appl. Phys.* **34,** 813–818 (1963).
14. Zhang, J. *et al.* Continuous metal plasmonic frequency selective surfaces. *Opt. Express* **19,** 23279–23285 (2011).
15. Vorobyev, A. Y. & Guo, C. Enhanced absorptance of gold following multipulse femtosecond laser ablation. *Phys. Rev. B* **72,** 195422 (2005).
16. Vorobyev, A. Y. & Guo, C. Colorizing metals with femtosecond laser pulses. *Appl. Phys. Lett.* **92,** 041914 (2008).
17. Wang, X., Zhang, D., Zhang, H., Ma, Y. & Jiang, J. Z. Tuning color by pore depth of metal-coated porous alumina. *Nanotechnology* **22,** 305206 (2011).
18. Chattopadhyay, S. *et al.* Anti-reflecting and photonic nanostructures. *Mater. Sci. Eng. R* **69,** 1–35 (2010).
19. Lewis, N. S. Toward cost-effective solar energy use. *Science* **315,** 798–801 (2007).
20. Hilfiker, J. N. *et al.* Survey of methods to characterize thin absorbing films with spectroscopic ellipsometry. *Thin Solid Films* **516,** 7979–7989 (2008).

Acknowledgements

We acknowledge helpful discussions with J. Lin, N. Yu and J. Choy, and thank J. Deng and R. Sher for assistance with the measurements. We also thank L. Liu and E. Grinnell for assistance in photography. The fabrication and some of the measurements were performed at the Harvard Center for Nanoscale Systems, which is a member of the National Nanotechnology Infrastructure Network. We thank E. Mazur for access to his spectrophotometer. This research is supported in part by the Air Force Office of Scientific Research under grant number FA9550-12-1-0289. M. Kats is supported by the National Science Foundation through a Graduate Research Fellowship.

Author contributions

M.A.K. developed the concept, performed the calculations and fabricated the samples. M.A.K. and R.B. characterized the samples and performed the measurements. M.A.K., R.B., P.G. and F.C. analysed and interpreted the data and implications. M.A.K., R.B. and F.C. wrote the manuscript. F.C. supervised the research.

Additional information

Supplementary information is available in the online version of the paper. Reprints and permissions information is available online at www.nature.com/reprints. Correspondence and requests for materials should be addressed to F.C.

Competing financial interests

The authors declare no competing financial interests.

nature materials

SUPPLEMENTARY INFORMATION

DOI: 10.1038/NMAT3443

Nanometre optical coatings based on strong interference effects in highly absorbing media

Mikhail A. Kats, Romain Blanchard, Patrice Genevet, and Federico Capasso*

School of Engineering and Applied Sciences, Harvard University, Cambridge, Massachusetts 02138, USA

*capasso@seas.harvard.edu

DOI: 10.1038/NMAT3443

Additional photographs of samples

For visual clarity, we include an additional photograph of the samples shown in Fig. 4 in the main text in Fig. S1. The photograph was taken on a black background with diffuse white light illumination.

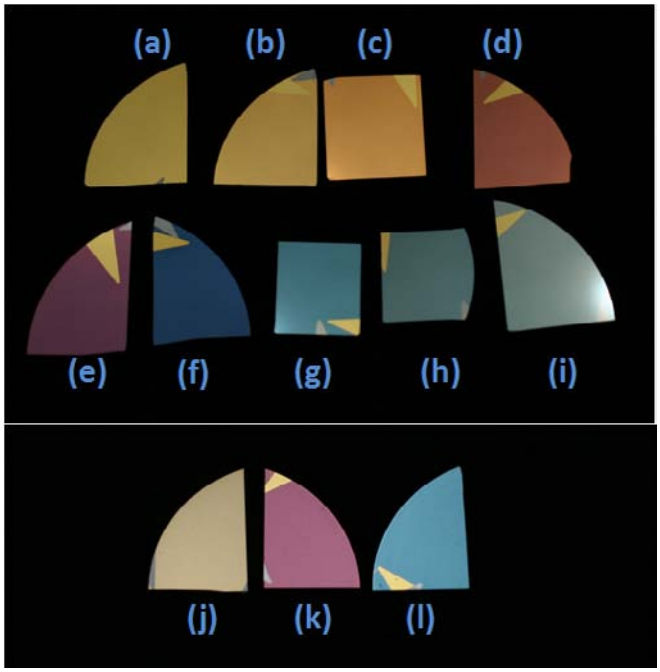

Figure S1. Another photograph of the samples shown in Fig. 4. (a) Bare Au surface before Ge deposition. The optically-thick (150 nm) Au film was deposited on a polished Si substrate (b-i) Colors formed by coating Au with 3 nm, 5 nm, 7 nm, 10 nm, 15 nm, 20 nm, 25 nm, and 30 nm of Ge, respectively. (j) 150 nm of Au deposited on a rough (unpolished) Si substrate. (k, l) 10 nm and 20 nm of Ge deposited over 150 nm of Au, on a rough Si substrate.

Partial-wave explanation of resonance

In this section, we focus on the physical mechanism of the ultra-thin film resonance and explain the conditions in which it can occur. We begin by analyzing the total reflectivity from a structure like that in Fig. 1(b), where medium 2 has complex refractive index $n + ik$ and medium 3 is a PEC. We plot the reflectivity at $\lambda = 532$ nm as a function of n and k, and find that for a film with $h = 10$ nm the reflectivity stays close to 1 for all values of (n, k) from 0 to 5, but for $h = 50$ nm a zero in reflectivity occurs at 2.81 + 0.61i, which corresponds roughly to the $\lambda/4n$ (quarter-wave) film (Fig. S2). This can be understood as a critical coupling condition to the lossy asymmetric

Fabry-Perot cavity formed inside the film [S1] [S2]. No absorption resonance exists for a film thinner than this with a PEC substrate.

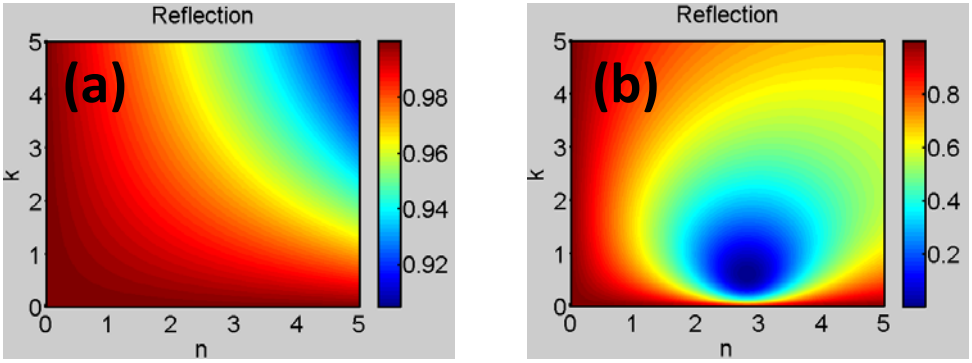

Figure S2. (a, b) Reflectivity for a film with complex index $n + ik$ and h = 10 nm and 50 nm, respectively, on a PEC substrate, at λ = 532 nm.

When the conductivity of the substrate becomes finite, however (as is the case for metals at visible frequencies (Fig. 1(d)), the situation changes significantly. For example, in Fig. S3 we plot the reflectivity vs (n, k) of the films given that the substrate is Au at λ = 532 nm (n_3 = .44 + 2.24i). We observe that when the index of the film is 4.3+0.71i, the reflectivity drops to zero even though the film thickness is only 10 nm, corresponding to ~$\lambda/12n$.

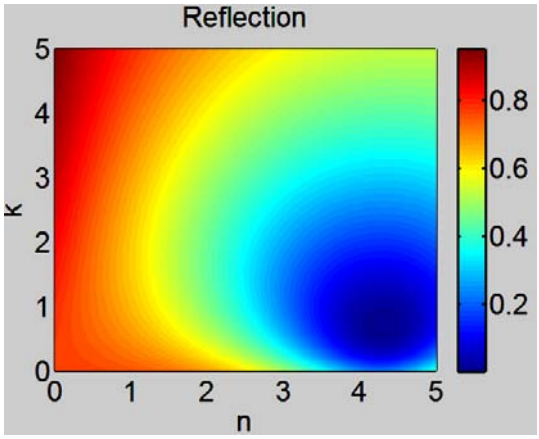

Figure S3. Reflectivity for a film with complex index $n + ik$ and h = 10 nm on a gold substrate at λ = 532 nm.

DOI: 10.1038/NMAT3443

To better understand the mechanism leading to the reflectivity minimum at 4.3+0.71i, we expand Eqn. 1 into partial waves to get $r = \sum_{m=0}^{\infty} r_m$ where $r_m = t_{12} r_{23}^{\,m} r_{21}^{\,(m-1)} t_{21} e^{2mi\beta}$ for m > 0 and $r_{pq} = (\tilde{n}_p - \tilde{n}_q)/(\tilde{n}_p + \tilde{n}_q)$, $t_{pq} = 2\tilde{n}_p/(\tilde{n}_p + \tilde{n}_q)$, and $r_0 = r_{21}$. With this formulation, we can plot the reflectivity taking into account only the first *m*' partial waves to see how the reflectivity evolves as more and more partial waves are included. We do this in Fig. S4 (a) and (c), where we assume that the substrate is a PEC or Au at 532 nm, respectively, h = 10 nm, and n_2 = 4.3 + ik where k can vary from 0 to 2.1 (see legend). We see that in the PEC case the final reflectivity is close to 1 for all values of k. The partial reflectivity goes above 1 when only the first 1-2 secondary waves are taken into account, but the value drops back down below 1 when the other partial waves are included, preserving energy conservation. In the case of Au, however, the reflectivity changes significantly with changing k, even reaching precisely 0 at approximately k = 0.7. Note that for all cases with significant loss (k >> 0) the partial reflectivity reaches its final value of after only 3-4 partial waves are accounted for (corresponding to 3-4 passes through the lossy medium).

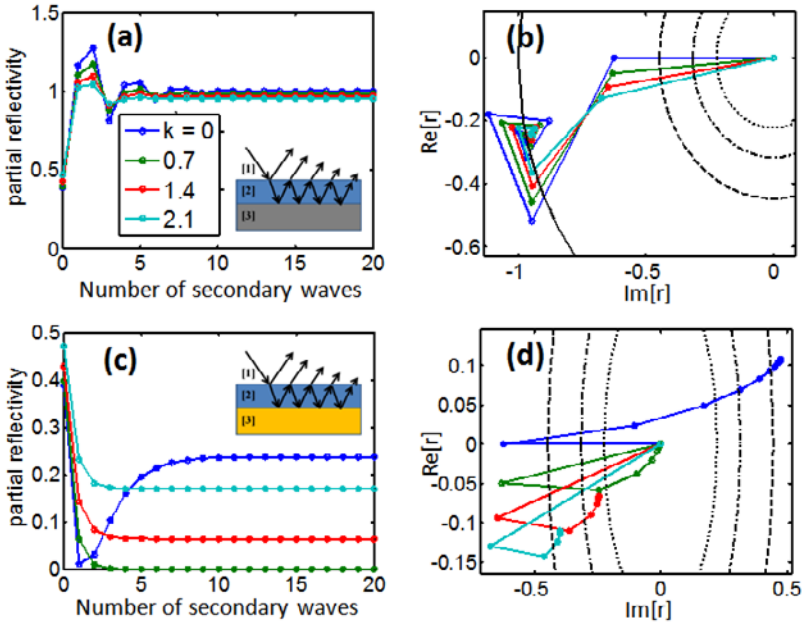

Figure S4. (a) Partial reflectivity from the sample taking into account the initial reflection between mediums 1 and 2, and also 0, 1, ... secondary partial waves where the first partial wave comes from a single round trip through medium 2, the second from two round trips, etc. The substrate is a perfect electric conductor (PEC), with $n_3 = \infty + i\infty$. Medium 2 has index 4.3 + ik, where k is given in the legend

of (b), λ = 532 nm, and h = 10 nm. (b) Phasor diagram corresponding to (a), showing graphically how all values of k within the range of 0 - 2.1 lead to roughly the same overall reflection coefficient R (close to 1). The circles each represent a particular reflectivity (R = 1: solid line, R = 0.2: dashed line, R = 0.1: dot-dashed line, R = 0.05: dotted line), which is reached if the phasor trajectory terminates on a particular circle. (c) Partial reflectivities as in (a), but with n_3 = 0.44 + 2.24i, the complex index of Au at 532 nm. (d) Phasor diagram corresponding to (c). The resulting values of R can be read off by using the circles as a reference. In particular, the k = 0.7 trajectory ends up at the origin, yielding R = 0.

Since the partial wave amplitudes are all complex quantities, we can plot them in the complex plane, where they are represented as vectors (referred to as "phasors") (Fig. S4 (b, d)). The first phasor r_0 begins at the origin, r_1 begins at the end of r_0, etc. The total reflectivity R is the magnitude-squared of the final value of the phasor trajectory in the complex plane (R is identically zero if the trajectory returns to the origin). In the case of the PEC substrate, the first few partial waves all move away from the origin, indicating constructive interference and therefore a large final value of R (Fig. S4(b)). With the Au substrate, however, the phasor trajectory makes a sharp turn after the first partial wave, a result of the near-zero phase shift that the light experiences reflecting from a lossy dielectric into a low-optical-conductivity metal (such as Au at 532 nm), opening the possibility that the complex sum of the secondary partial waves could partially or totally cancel r_0.

In the phasor diagrams in Fig. S4(b, d), we drew circles centered on the origin corresponding to reflectivities R = 1, 0.2, 0.1, and 0.05 (solid line, dashed line, dot-dashed line, dotted line, respectively). This allows us to visually identify the reflectivity by using the circles as references; for example, since the k = 1.4 (red) trajectory terminates between the dotted and dot-dashed circles, we know that R is between 0.05 and 0.1. We see that varying k results in a wide range of reflectivities. In particular, the k = 0.7 trajectory terminates precisely at the origin, resulting in R = 0 (corresponding to 100% absorption). The reflectivity minimum in n-k space is very broad (Fig. S3), so even when the values do not precisely match those of the minimum-reflectivity condition, a significant absorption resonance can still be observed. This is what happens for evaporated Ge films in our experiments (Fig. 2(b, c)), which at 532 nm correspond to the cyan curve in Fig. S4(a). We note that while the R = 0 condition cannot be achieved with the Ge/Au material system in the visible at normal incidence due to the limited degrees of

DOI: 10.1038/NMAT3443

freedom (k_2 and n_2 can be tuned by controlling the incident wavelength, but not independently of each other), such a condition can be found for some incident angles. For example, the reflectivity in Fig. 3(b) drops to 0 for $\theta \sim 70°$ and $\lambda \sim 535$nm.

Absorption in the substrate

We performed analytical calculations in the same manner as in the main text (following the textbook matrix method such as that of ref. [6]) to obtain separate plots of absorption in the Ge layer and absorption in the Au substrate (Fig. S5(b) and (c), respectively). We observe that the vast majority of the absorbed power is dissipated in the Ge film, with only a small fraction of the light dissipated in the underlying Au substrate.

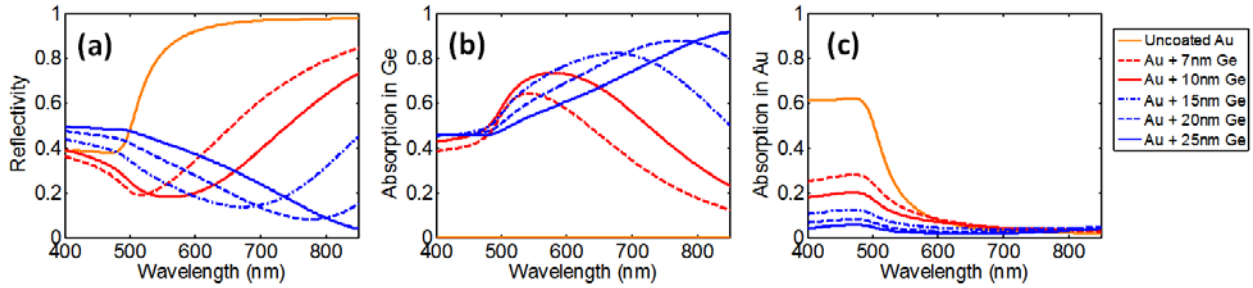

Figure S5. (a) Calculated reflectivity spectra from the Au/Ge geometry for various thicknesses of Ge given a 7° angle of incidence and mixed polarization (reproduced from Fig. 2(c) in the main text). (b, c) Calculated fractions of the total power absorbed in the Ge film and in the underlying Au substrate, respectively, corresponding to the reflectivity spectra in (a).

Surface profile of samples

We performed AFM measurements on some of the bare and coated substrates to obtain an estimate of the surface roughness post-deposition. For the films deposited on polished Si wafers (Figs. 2, 3, and 4(a-h) in the main text), we found that the RMS roughness was ~1.24 nm for the uncoated Au sample, ~0.47 nm for the sample coated with 7 nm of Ge, and ~0.37 nm for the sample coated with 20nm of Ge (Fig. S6). We also performed contact profilometer measurements on the samples deposited on the rough back-sides of Si wafers (Fig. 4(k-m) in main text), and found that the RMS roughness was ~680 nm, with the lateral feature size of approximately 5-10 μm.

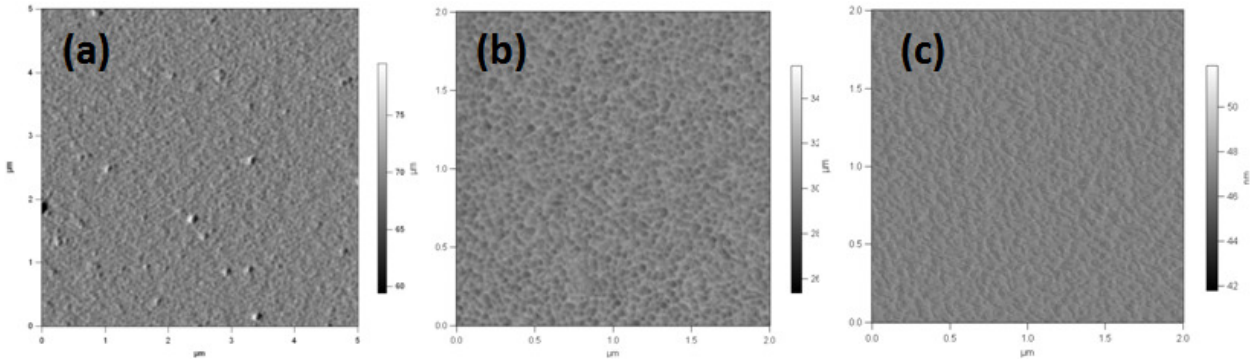

Figure S6. AFM images of 5 μm x 5 μm patches of the uncoated Au sample (a), the Au sample with 7nm of Ge (b), and the Au sample with 20nm of Ge (c), all deposited on a polished Si substrate.

Stability of the films

Long-term stability of the highly-absorbing films may be a concern for some applications. In the case of our experiments, the measurements were within 1-2 days of the deposition, and the samples were then stored in gel-boxes outside of any cleanroom environment. No special care was taken to protect the samples, which were also periodically completely exposed to ambient conditions. We observed no perceptible change in the colors of the samples over a four month period, indicating that they are relatively stable. We also performed another set of reflectivity measurements corresponding to that of Fig. 3 on the same sample, and observed very little change over these four months (Fig. S7).

DOI: 10.1038/NMAT3443

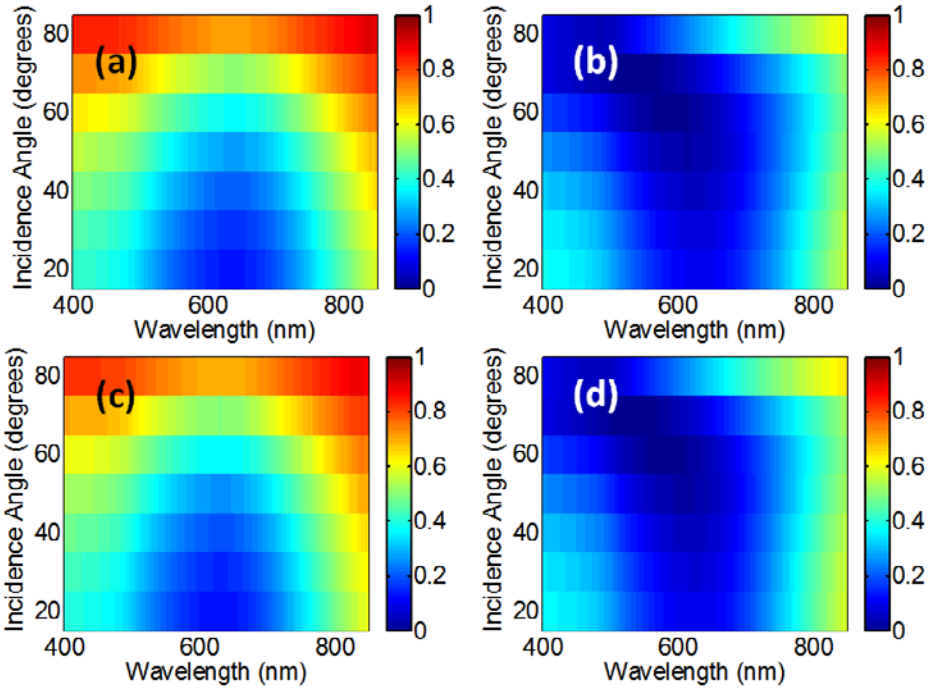

Figure S7. (a, b) Experimental reflectivity spectra for s- and p-polarization, respectively, for angles of incidence from 20° to 80° for an Au film coated with 15 nm of Ge, as taken one day after the deposition of Ge. This is the same data as presented in Fig. 3(a, b). (c, d) Experimental reflectivity spectra corresponding to those in (a, b), taken ~4 months after the deposition.

For long-term stability, however, a variety of methods may be required to passivate and protect the semiconductor surface. If Ge is used as in the present work, then this can be achieved by chemical passivation methods (e.g. sulfide functionalization) [S3], which will not significantly affect the optical properties of the films. Alternatively, a capping layer may be deposited on top of the semiconductor to protect against chemical or mechanical damage. One possibility is sputtered hydrogenated amorphous germanium (a-Ge:H), which has been used to protect, for example, Ge-based nuclear radiation detectors and can be tens of nanometers thick [S4] [S5]. Another is the hard carbon coating, also known as the diamond-like coating (DLC), which adheres well to germanium and silicon, and is extremely resistant to both chemical and abrasive environments [S6] [S7].

A capping layer with a thickness of tens of nanometers or more may significantly affect the observed optical properties, depending on the optical properties of the material and its thickness.

To test this, we performed 4-layer transfer matrix calculations, including a 10 nm DLC layer on top of the Ge. This thickness was chosen because it was the thinnest DLC layer that was analyzed as a protective coating in ref. [S7], and the complex refractive index was interpolated from the data provided in ref. [S6]. The resulting reflection spectrum was nearly unaltered (Fig. S8). A thicker layer may change the reflectivity properties significantly; however based on our calculations the ultra-thin absorption resonances can still be successfully designed. In fact, the capping layer can be seen as an additional degree of freedom in the design of these thin optical coatings.

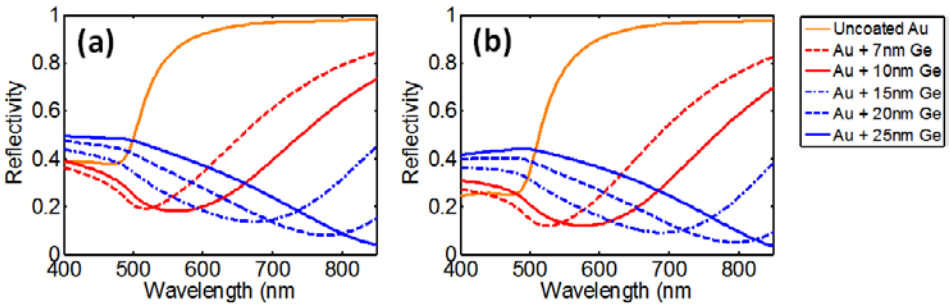

Figure S8. Normal incidence reflectivity calculations of a Au/Ge system for Ge thicknesses between 0 nm and 25 nm as in Fig. 2(c) in the main text with (a) no protective coating and (b) a 10 nm diamond-like coating (DLC)

Equivalent reflecting material

The following point was raised by one of the referees: since the presently-demonstrated semiconductor layers have a thickness much smaller than the wavelength of light, an equivalent semi-infinite medium can be defined which has the same reflectivity spectra as the combined substrate/film structure for various angles of incidence.

To explore this, we used the concept of "input optical admittance or "surface optical admittance", which is sometimes used to analyze optical thin film assemblies (e.g. ref. [1] in the main text). For any arbitrary collection of films, one can define a single surface admittance at an interface between medium 1 and medium 2, which takes into account the effect of all of the layers underneath (2, 3, 4, etc..). This is analogous to defining a single electrical admittance (or, equivalently, impedance) for a circuit comprising many elements. For materials without a magnetic response (permeability $\mu = 1$, which is usually small at optical frequencies (ref. [1])),

DOI: 10.1038/NMAT3443

the surface optical admittance is directly proportional to a surface refractive index, and we will limit ourselves to this case.

For example, we analyzed the structure comprising an Au substrate with 15 nm of Ge (blue dot-dashed curve in Fig. 2, and the data of Fig. 3 in the main text) and calculated the normal incidence reflectivity (Fig. S9(a)) as well as the surface refractive index (Fig. S9(b)). The extracted values for the surface refractive index (n and k) are such that one could reasonably imagine a real material (or a metamaterial) with these parameters. We used these values of n and k to calculate the reflectivity at several oblique angles for both s- and p-polarization, and compared them to the actual calculated reflectivities from the layered system (Fig. S10).

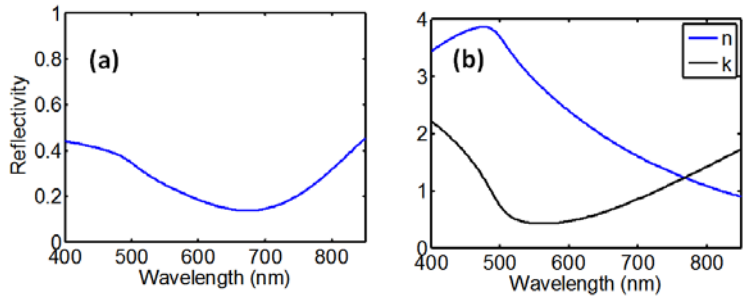

Figure S9. Calculated reflectivity for normal incidence from a gold surface coated with 15 nm of Ge (a) and extracted surface refractive index (b)

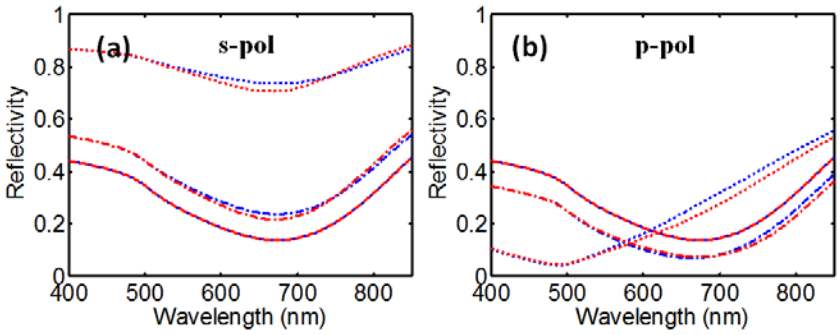

Figure S10. Calculated reflectivity spectra for oblique incidence ((a) s-polarization and (b) p-polarization) from the layered geometry (blue) and from a flat infinite half-space with complex refractive indices (n, k) given in Fig. S9(b) (red). The reflectivity data for $\theta = 0°$ is shown with the dashed curves, for $\theta = 40°$ with the dot-dashed curves, and the $\theta = 80°$ with the dotted curves.

The match is not perfect, which means that strictly speaking one cannot define a homogeneous semi-infinite medium which is completely equivalent to the layered system when looking at the reflection properties. However, the reflectivity curves actually match reasonably for both p- and s- polarization for all incident angles, indicating that it is possible to define a semi-infinite medium which *nearly* reproduces the optical properties of the layered system. This means that, to an approximation, one can also define quantities such as the pseudo-Brewster angle [S8] for our layered surface.

Supplementary references

[S1] H. A. Haus, Waves and Fields in Optoelectronics. (Prentice-Hall, New Jersey, 1984)

[S2] R. H. Yan, R. J. Simes, and L. A. Coldren, "Surface-normal electroabsorption reflection modulators using asymmetric Fabry-Perot structures", IEEE Journal of Quantum Electronics 27, 1922 (1991)

[S3] P. W. Loscutoff and S. F. Bent, "Reactivity of the germanium surface: chemical passivation and functionalization", Annual Review of Physical Chemistry 57, 467-495 (2006)

[S4] W. L. Hansen, E. E. Haller, G. S. Hubbard, "Protective surface coatings on semiconductor nuclear radiation detectors", IEEE Transactions on Nuclear Science NS-27, 1 (1980)

[S5] Hansen et al, "Germanium detector passivated with hydrogenated amorphous germanium", U.S. Patent 4589006

[S6] Tydex Optics, Hard Carbon Coating Datasheet, http://www.tydexoptics.com/materials1/coatings/dlccoatings/

[S7] M. Alaluf, J. Appelbaum, L. Klibanov, D. Brinker, D. Scheiman, N. Croitoru, "Amorphous diamond-like carbon films -- a hard anti-reflecting coating for silicon solar cells", Thin Solid Films 256 (1995)

[S8] R. M. A. Azzam, "Maximum minimum reflectance of parallel-polarized light at interfaces between transparent and absorbing media", JOSA 73, 7 (1983)